Hindawi Publishing Corporation
Advances in Tribology
Volume 2012, Article ID 163575, 9 pages
doi:10.1155/2012/163575

Research Article

Some Experimental and Simulation Results on the Dynamic Behaviour of Spur and Helical Geared Transmissions with Journal Bearings

R. Fargère[1, 2] and P. Velex[2]

[1] *Département Dynamique des Structures, DCNS Research, Centre d'Expertise des Structures & Matériaux Navals, 44 620 La Montagne, France*
[2] *LaMCoS, UMR CNRS 5259, INSA Lyon, Université de Lyon, Bâtiment Jean d'Alembert, 20 avenue Albert Einstein, 69 621 Villeurbanne Cédex, France*

Correspondence should be addressed to P. Velex, philippe.velex@insa-lyon.fr

Received 11 July 2012; Accepted 15 November 2012

Academic Editor: Benyebka Bou-Saïd

Copyright © 2012 R. Fargère and P. Velex. This is an open access article distributed under the Creative Commons Attribution License, which permits unrestricted use, distribution, and reproduction in any medium, provided the original work is properly cited.

Some interactions between the dynamic and tribological behaviour of geared transmissions are examined, and a number of experimental and simulation results are compared. A model is introduced which incorporates most of the possible interactions between gears, shafts and hydrodynamic journal bearings. It combines (i) a specific element for wide-faced gears that includes the normal contact conditions between actual mating teeth, that is, with tooth shape deviations and mounting errors, (ii) shaft finite elements, and (iii) the external forces generated by journal bearings determined by directly solving Reynolds' equation. The simulation results are compared with the measurement obtained on a high-precision test rig with single-stage spur and helical gears supported by hydrodynamic journal bearings. The experimental and simulation results compare well thus validating the simulation strategy both at the global and local scales.

1. Introduction

Despite their inherent drawbacks such as the generation of noise, vibrations, and contact failures, geared systems are commonly used in mechanical transmissions for their high efficiency and power transmission capacity. In some applications for which noise can be a critical issue, such as marine propulsion, journal bearings offer a viable alternative to rolling element bearings because of their interesting damping properties which, however, can be counterbalanced by instabilities and nonlinear phenomena. From a modelling point of view, the coupling of all these mechanical parts requires simultaneous treatment of the structural problem associated with the shaft lines and the contact problems not only between the mating teeth but also at the shaft/bearing interfaces. Each of these individual mechanical topics has generated a vast body of literature over the years. Concerning journal bearings, the first seminal papers date back to the second half of the 20th century [1–4], and a valuable synthesis can be found in [5] for the basic phenomena. The influences of thermal effects [6], oil injection properties, lubricant rheology, shaft misalignments, [7] and the local elastic deflections on shafts and bearings [8] have been studied over the past 40 years and are, today, correctly mastered; however the computational costs can be prohibitive, particularly in an industrial context. On the other hand, gear dynamics has been extensively analyzed in recent decades based on increasingly refined models [9, 10] which usually combine rigid gears, discrete stiffness, and damping elements [11, 12]. Later, time-varying mesh stiffness along with mounting errors and tooth shape modifications have been considered [13, 14], and gear body deflections have been introduced via shaft [15] or 3-dimensional solid finite elements.

Several models dealing with the interactions between gears and bearings can be found in the literature, but, most of them, do not consider either gear mesh or bearing nonlinearities. Theodossiades and Natsiavas [17] and Chen et al. [18] used a simplified mesh interface coupled with

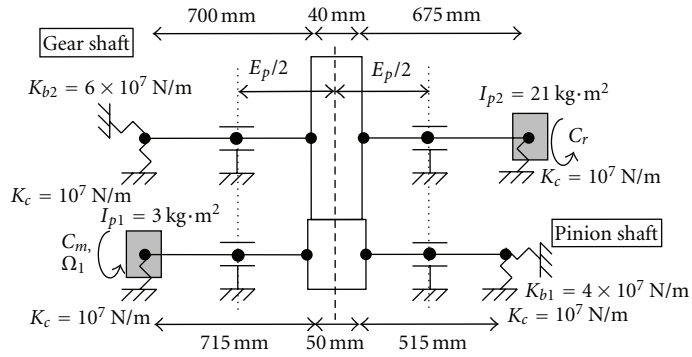

Figure 1: Model of the test-rig.

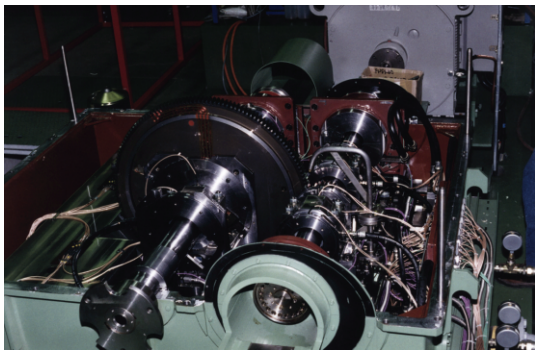

(a) Photo of the test-rig

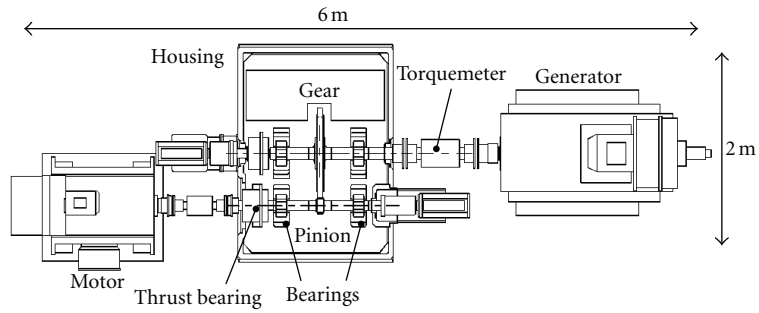

(b) Schematic representation of the test rig

Figure 2: Presentation of the test rig.

the nonlinear properties of journal bearings. Baud and Velex [16] simulated journal bearings via stiffness and damping coefficients while employing the sophisticated gear model presented in [14]; a number of comparisons with the evidence from a test rig were presented. More recently, journal bearing-gear nonlinear interactions have been studied by Baguet and Jacquenot [19] who coupled gear and shaft elements along with bearing forces calculated using a multigrid method.

The present work is in the continuation of [19] but a more refined simulation of the interactions is proposed which relies on the original mesh model of [15], an efficient bearing approximation [6, 20], and introduces updated centre-distance, pressure angle, misalignments, and mesh characteristics in relation to the positions of the shafts in the bearings. Bearing and meshing models have been chosen to deal with most of the possible parameters and phenomena met in real ship transmissions: wide-faced gear bodies with profile modifications (necessary for high power transmission and silent running) and finite length journal bearing model with oil injection area, cavitation, and thermal effects. The model is fully configurable in terms of geometry and running conditions, and its results are compared with the experimental findings of Baud and Velex [16]. The comparisons deal with tooth contacts (dynamic amplification) and the bearing behaviour (steady-state position) for various geometries and running conditions.

2. Mechanical Model

A hybrid model has been developed which incorporates the gear simulation presented in [15], in which a pinion and a gear are assimilated to two deformable shafts linked by a time-varying series of nonlinear stiffness elements distributed along the potential contact lines on the base plane. The shafts are modelled by two-node Timoshenko beam elements which account for traction, torsion, and bending whereas the other components such as couplings and load machines, are represented by lumped stiffness and/or inertia elements. Following [21], the bearings contribute via external force vectors calculated by solving Reynolds' equation in relation to the instant shaft positions and velocities in each bearing [5].

The mesh stiffness elements are evaluated from the bidimensional results of Weber and Banaschek [22] for structural deflections (tooth bending, base) and Lundberg's formula for contact compliance [23]. As tooth flanks move relative to each other, the contact geometries and global mesh stiffness are updated based on rigid-body displacements. Tooth friction is neglected, and only the normal compressive forces are considered. Any given stiffness element which is not in compression is set to zero (e.g., in the case of partial contacts on tooth flanks) and the gear stiffness matrix and forcing terms are recalculated until convergence is achieved. It is also checked that there is no compression outside

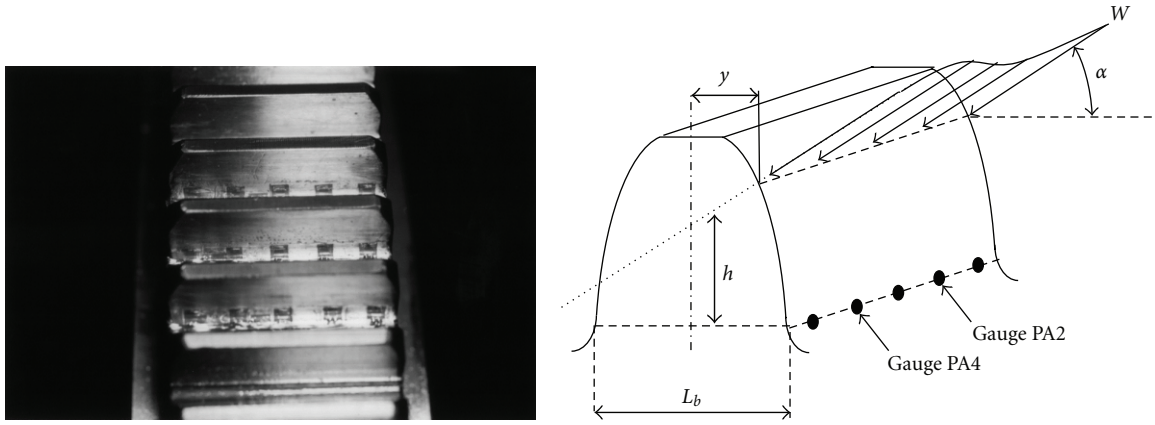

(a) Strain gauges at the fillet of the spur gear teeth

(b) Gauge locations and parameters for the calculation of tooth root stresses

FIGURE 3: Gauges at the roots of the teeth.

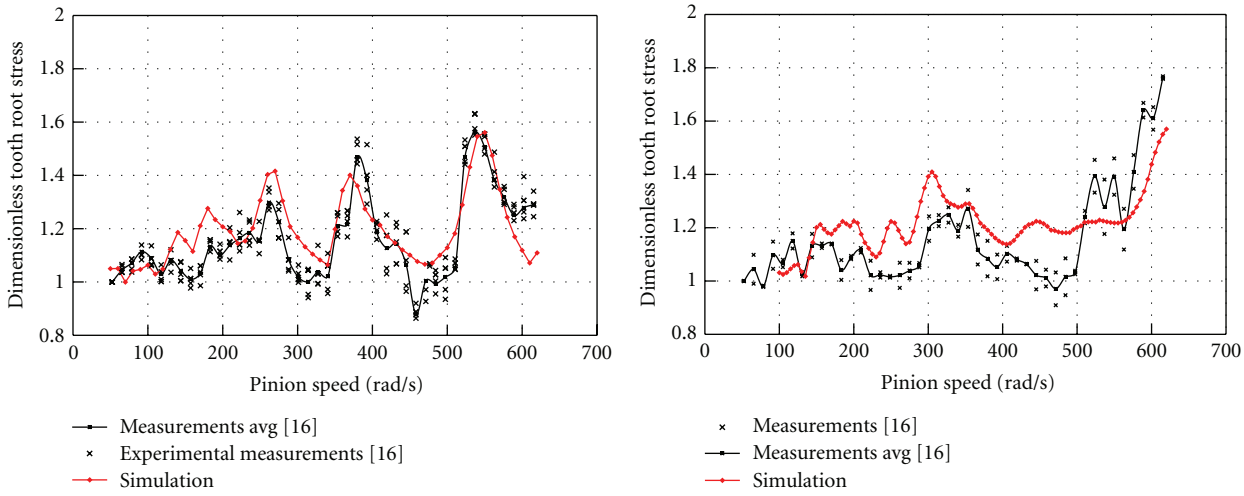

(a) (b)

FIGURE 4: Comparisons between the simulated and measured local dynamic coefficient with $C_r = 1540\,\text{N}\cdot\text{m}$ (a) maximum bearing spacing; and (b) minimum bearing spacing.

the contact area. Further details about the mathematical developments can be found in [14, 15].

Bearing reactions are considered as external lumped forces acting at one shaft node which are calculated by integrating the pressure field p over the bearing area. The classic method of Rhode and Li [20] (also known as the generalised short-bearing theory) is used which relies on the hypothesis of a parabolic pressure variation in the axial direction so that the remaining unknown is the circumferential pressure distribution. By so doing, the size of the problem is considerably reduced, and systematic parameter analyses are possible. A finite difference scheme combined with a Gauss-Seidel method is employed to find the angular pressure distribution. This method is very accurate for bearings such that the ratio $L/D \leq 1$ (with L, the bearing length, and D, the shaft diameter) can deal with realistic boundary conditions for oil injection and cavitation (Reynolds' conditions $p(\theta) = 0$ and $\partial p/\partial\theta = 0$ at the rupture abscissa) when using Christopherson's algorithm [24]. The bearing model is coupled with (i) a global thermal model [5] in which the temperature increase ΔT is calculated by equating a percentage of the heat generated by the fluid shearing with the heat ejected at the bearing edges, along with (ii) a fluid circulation model [6] so that the lubricant density and viscosity can be updated separately in each bearing using the empirical laws given in [25].

The coupling of all the system components leads to the parametrically excited nonlinear equations of motion of unknown $\mathbf{X}$:

$$[\mathbf{M}_S + \mathbf{M}_I]\ddot{\mathbf{X}} + [\mathbf{C}]\dot{\mathbf{X}} + [\mathbf{K}_S + \mathbf{K}_M(t, \mathbf{X}) + \mathbf{K}_C]\mathbf{X} = \mathbf{F}_{\text{ext}}(t) + \mathbf{F}_b(\mathbf{X}_R, \mathbf{X}, \dot{\mathbf{X}}) + \mathbf{F}_M(t, \mathbf{X}) - [\mathbf{K}_C]\mathbf{X}_R, \quad (1)$$

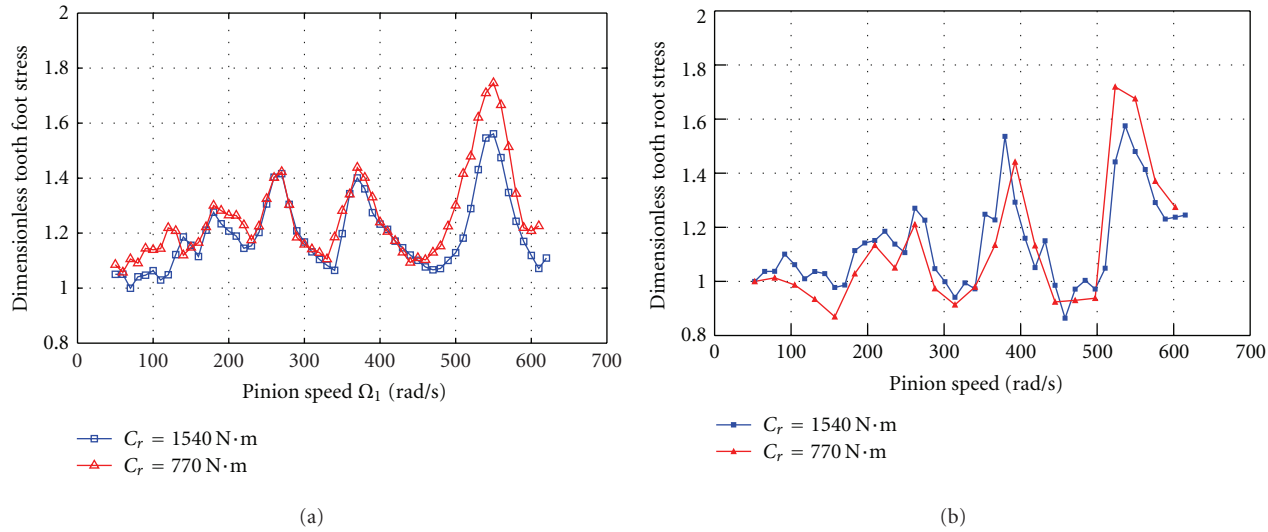

FIGURE 5: Effect of a load variation on the dimensionless tooth root stress, gauge PA2, (a) simulation results, (b) measurements [16].

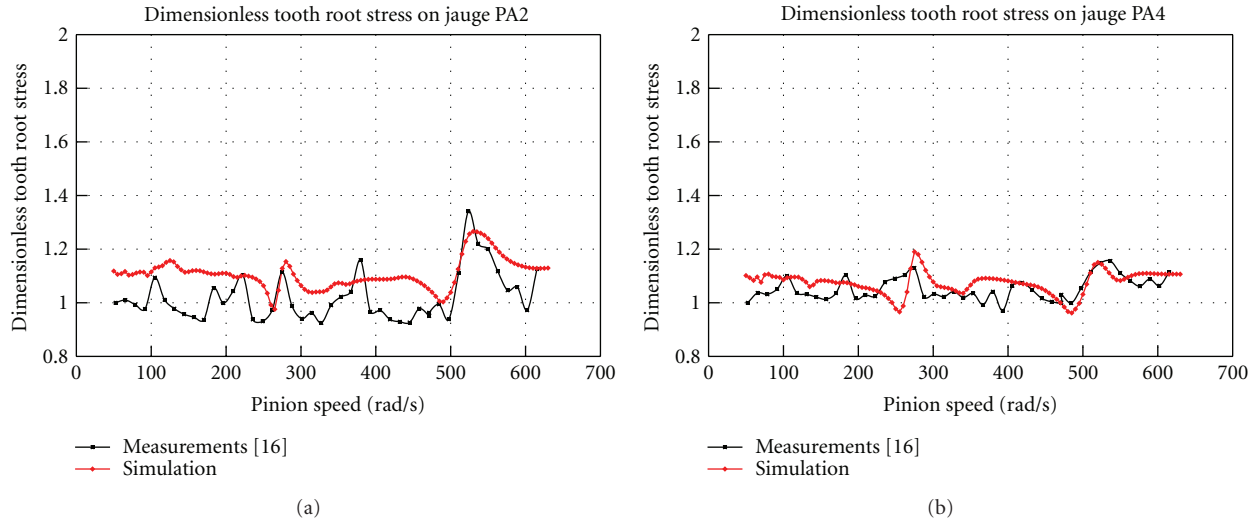

FIGURE 6: Comparisons between the simulated and measured dimensionless tooth root stress (helical gear case), with $C_r = 1540\,\text{N}\cdot\text{m}$ and maximum bearing spacing, (a) on gauge PA2, (b) on gauge PA4.

where $[\mathbf{M_S}]$ and $[\mathbf{M_I}]$ are, respectively, the mass matrix of the shafts and additional inertial elements and $[\mathbf{C}]$ is the damping matrix.

Index "X" in stiffness matrices $[\mathbf{K}_X]$ and external force vectors $\mathbf{F}_X$, respectively, refers to shafts for "S," gear mesh for "M," external couplings for "C" and bearings for "b." $\mathbf{F}_{\text{ext}}$ contains the equivalent nodal forces corresponding to the external torques, mass imbalance, and weight of the parts.

$\mathbf{X}_R$ represents the rigid-body displacement field which is used as the datum for the DOFs, mesh geometry, and shaft misalignments (deviation and inclination).

The nonlinear system (1) is directly solved by combining a Newmark scheme, a Newton-Raphson algorithm, and an iterative process aimed at updating the dynamic characteristics of the meshing process. At each time step, the bearing reaction forces are calculated by integrating the pressure distribution as opposed to the classic linear theory which relies on first order expansions in the vicinity of the static solution and leads to stiffness and damping dynamic coefficients.

The initial conditions are $\dot{\mathbf{X}}(t=0) = \mathbf{0}$ and $\mathbf{X}(t=0) = \mathbf{X_0}$ with $\mathbf{X}_0$, solution to

$$[\mathbf{K}_S + \overline{\mathbf{K}_M} + \mathbf{K}_C]\mathbf{X}_0 = \mathbf{F}_{\text{ext}} + \mathbf{F}_{b0}(\mathbf{X}_R, \mathbf{X}_0) - [\mathbf{K}_C]\mathbf{X}_R, \quad (2)$$

where $[\overline{\mathbf{K_M}}]$ is an averaged mesh stiffness matrix.

The static equilibrium is found by iterating with updated values of oil viscosity, density, and conductivity in each bearing until the running temperature of each bearing has converged.

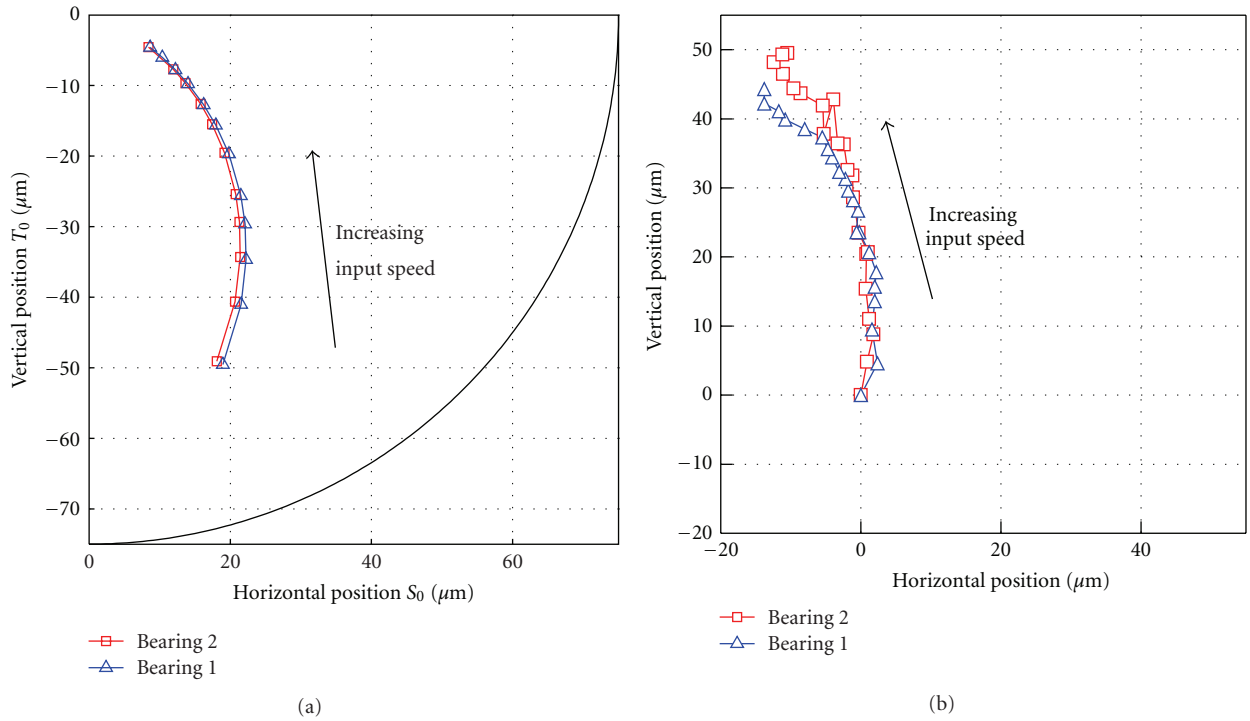

FIGURE 7: Comparisons of the simulated (a) and measured [16] (b) positions of the shaft centre inside the bearings at static equilibrium, spur gear set, $C_r = 1540\,\text{N}\cdot\text{m}$, $50\,\text{rad/s} < \Omega_1 < 700\,\text{rad/s}$.

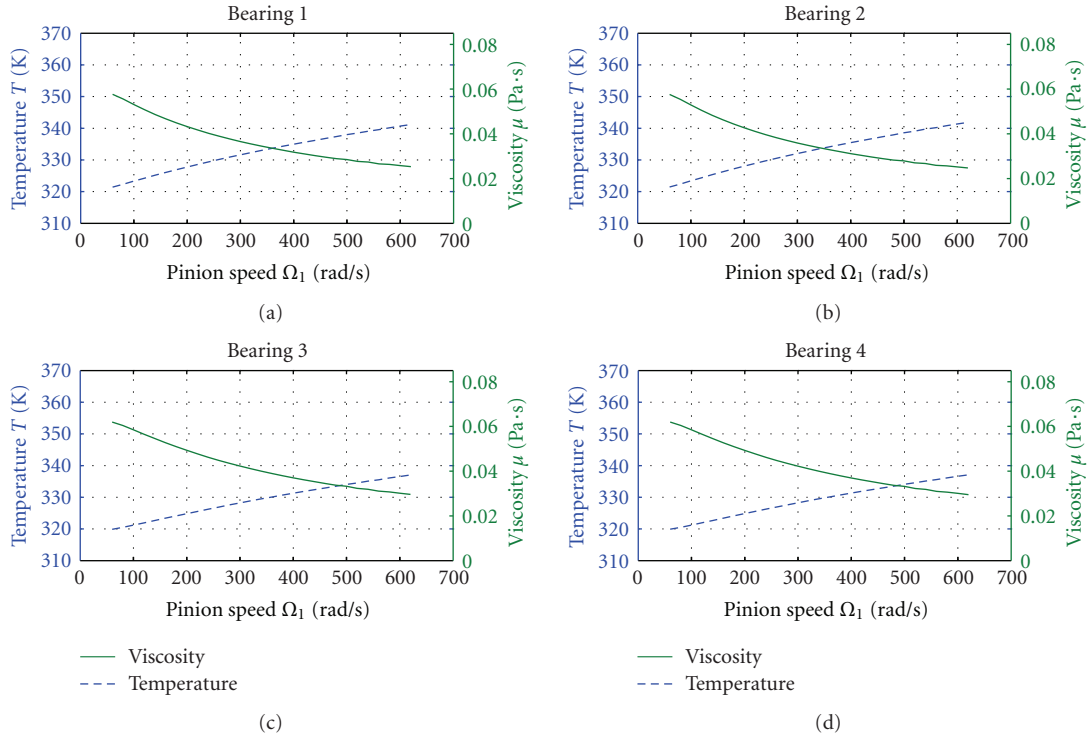

FIGURE 8: Variations of the bearing viscosities and temperatures with the input speed (spur gear se) $C_r = 1540\,\text{N}\cdot\text{m}$, $50\,\text{rad/s} < \Omega_1 < 700\,\text{rad/s}$.

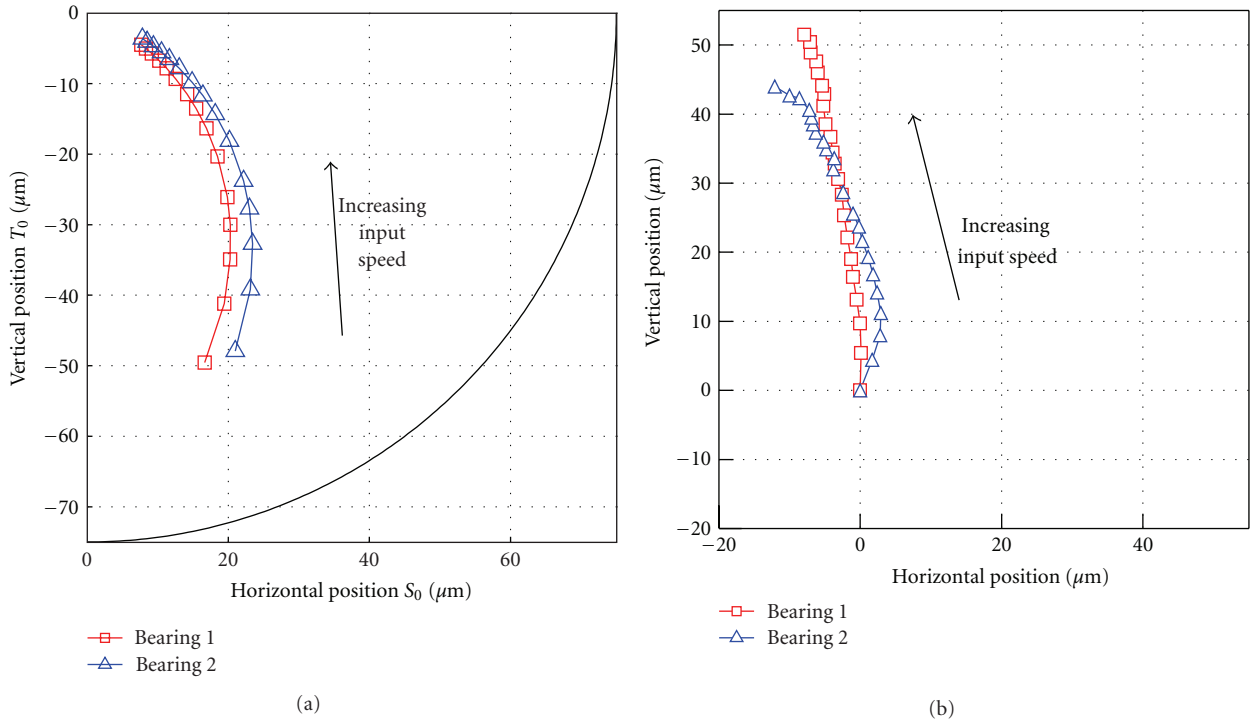

FIGURE 9: Comparisons of the simulated (a) and measured [16] (b) position of the shaft centre inside the bearings at static equilibrium (helical gear set) $C_r = 1540\,\text{N}\cdot\text{m}$, $50\,\text{rad/s} < \Omega_1 < 700\,\text{rad/s}$.

3. Test Rig and Simulation

The test rig represented in Figure 1 and Figures 2(a) and 2(b) consists in a single-stage spur or helical geared system with parallel shafts resting on four hydrodynamic journal bearings which are fixed to the pedestal. The reduction unit is mounted on a cast iron base which is fixed to a reinforced concrete block lying on springs and dampers. The shafts were made to close tolerances, and particular care was taken in the manufacture of the test rig in order to be consistent with the accuracy of the gears (ISO precision grade 4, close to those used in ship reducers). The gears are jet lubricated from the oil circulating system common to the gears and the bearings (ISO VG 100). Thermostatic control is provided to keep the unit temperature as constant as possible, and the temperature of the oil in the sump is 45°C for all tests. Prior to recording data, the transmission was heated until oil temperatures and displacements of the base were stabilized. The pinion speed varies between 50 and 700 rad/s, and the maximum output torque is 4200 N·m. The spur and helical gear tooth profiles are modified by short linear tip relief of amplitude 20 μm (spur gears) and 13 μm (helical gears) over 20% of the nominal active profile on the pinion and the gear teeth. The peak to peak of cumulative pitch errors is within 10 μm for the pinion and 20 μm for the gear.

The instrumentation comprises (i) torque measurements, (ii) displacement probes which are positioned in pairs 90 degrees apart at four locations on each shaft, and (iii) strain gauges at the root of several teeth. Three successive teeth on the pinion are strain-gauged at the tensile side as shown in Figures 3(a) and 3(b) with four active gauges across the face width. Output signals are transmitted by leads cemented to the pinion/gear faces and inside the hollow shafts to two slip rings which transfer this data from the rotary to the stationary system.

From a modelling point of view, the profiles of all the teeth have been discretized to account for profile modifications and also pitch errors. Each shaft is decomposed into 5 finite elements (Figure 3) whose dimensions are specified in Tables 1, 2, and 3. A unique modal damping factor of 4% has been used to simulate the dissipation within the shaft-gear mesh subsystem whereas the damping provided by the journal bearings directly stems from the reaction forces determined from Reynolds' equation. In order to consider steady-state solutions, the simulations were launched over 128 mesh periods with 64 time steps per mesh period, and results were considered over the last 64 mesh periods only.

4. Comparisons between Experimental and Numerical Results

Using a classic beam approach for calculating root stresses and a thin-slice model for the teeth, the following approximate expression for slice i is introduced (Figure 3):

$$\sigma_{Ni} = \frac{M_{fi}}{I_G}\frac{L_b}{2}, \tag{3}$$

where $M_{fi} = W_i(h_i \cos\alpha_i - y_i \sin\alpha_i)$ is the bending moment due to the tooth load when isolating a slice i, I_G is the

Table 1: Gear data.

	Pinion	Gear
Tooth number	26	157
Face width (mm)	50	40
Helix angle (°)	0 and 12.5	
Module (mm)	4	
Pressure angle (°)	20	
Addendum coefficient	1.	1.
Dedendum coefficient	1.4	1.4
Profile shift coefficient	0.16	−0.16 (spur) and −0.14 (helical)
Center distance (mm)	366 (spur) and 375 (helical)	

Table 2: Shaft data.

	Pinion shaft	Gear shaft
Outer diameter (mm)	70	90
Inner diameter (mm)	30	30
Shaft length (mm)	1280	1415
Bearing distance to pinion/gear: E_p (mm)	640 max–320 min	
Young's modulus (MPa)	210 000	
Poisson's ratio	0.3	
Density (kg/m^3)	7 800	
Thrust bearing stiffness (N/m)	4×10^7	6×10^7 N
Elastic coupling stiffness (N/m)	1×10^7	

Table 3: Bearing (and lubricant) data.

	Pinion shaft	Gear shaft
Length (mm)	50	65
Radial clearance (μm)	75	55
Lubricant (mm)	ISO VG 100	
Kinematic viscosity (mm^2/s)	$v_{40} = 100$; $v_{100} = 11.384$	
Lubricant injection temperature (K)	318	
Oil injection	Axial groove opposed to load direction	

moment of inertia of the tooth section, and L_b is the root tooth thickness at the location where the stress is calculated/measured.

Note that for spur gears, index i can be omitted since it is supposed that there is no axial variation for perfectly aligned gears.

Denoting by σ_{REF} the reference fillet stress calculated for the total static normal load $C_m/R_b \cos\beta_b$ and $\alpha = \alpha_t$ passing by the pitch circle at the tooth centre line, a dimensionless tooth root stress is defined as

$$R_i = \frac{\sigma_{Ni}}{\sigma_{\text{REF}}}. \tag{4}$$

Considering the spur gear example, Figures 4(a) and 4(b) display a number of comparisons between the measured dimensionless root stresses [16] and the simulation results derived from the dynamic model and (3)-(4) for two bearing centre distances. A very good agreement is reported particularly when the distance between the bearings is maximal (640 mm). Contrary to the results in [16] where a simplified bearing model based on dynamic coefficients was used, the three major response peaks are correctly simulated (Figure 4(a)) suggesting that the bearings are influential on dynamic tooth root stresses or loads. Both the experimental and numerical results reveal that moving the bearings to the minimal centre distance of 320 mm significantly alters the dynamic load pattern on the teeth. The highest critical speed is shifted from 550 rad/s to more than 600 rad/s for the minimum bearing spacing which logically renders the system stiffer. In this configuration, the two secondary peaks do not clearly emerge any longer in the response curve but the speed range 300–350 rad/s exhibits significantly higher stress levels than the other speeds. This effect is correctly reproduced by the simulations even if the amplitudes are slightly larger than the experimental ones. It has to be noticed that the simulation curves are generally smoother, probably because of the limited number of shaft elements used in this model which, especially for the minimum bearing centre distance, cannot properly integrate the influence of the highest modes. The comparisons have been extended to two different nominal load levels, that is, a gear torque of $C_r = 1540$ and 770 N·m. It can be observed in Figure 5 that the experimental and numerical dynamic responses are only slightly affected, and, in particular, the tooth critical speeds are unchanged. Here again, the measurements and the simulation results compare very well.

The corresponding results for the helical gear pair ($\beta = 12.5°$) are shown in Figure 6 where the dimensionless maximum root stresses for two different gauges on the same tooth (PA2 and PA4 in Figure 3) are plotted against the pinion speed. As opposed to the spur gear example, the dynamic stress distribution appears as nonuniform across the tooth face width. The agreement between the experimental evidence and the simulations is still acceptable, and the variations with the gauge axial position are actually captured by the model. Generally speaking, the dynamic amplifications of the tooth fillet stress are less marked than for spur gears (a maximum of 1.3 versus 1.6 for the spur gear), and the main critical speed, around 540 rad/s, is only visible on the signals delivered by gauge 2.

Focusing on the bearing behaviour, Figure 7 shows the evolutions of the shaft centre positions with speed within the bearing clearance (black circle in the figure) for the spur gear case. Although only relative measurements have been performed, the experimental and numerical curves are similar both in terms of orientation and magnitude. In particular, a slight difference is reported between bearings 1 and 2 on the pinion shaft caused by the shaft asymmetry. The following conclusions can be drawn.

(i) The lubricant viscosity at each bearing is different depending on speed (Figure 8) since the actual temperature is modified by the running conditions (higher temperatures in bearings 1 and 2 where the rotational speed is higher than that at bearings 3 and 4).

(ii) The bearing reaction forces vary with speed in relation to the bearing position with respect to the couplings. However, their amplitudes remain close to half the mesh force, and their orientations correspond approximately to that of the base plane.

Similar results for the helical gear are presented in Figure 9 which prove that, in this case too, the experimental and numerical trajectories are in good agreement. It can be clearly observed that the shaft positions vary from one bearing to the next, even on the same shaft, and differ from what is found for the spur gear arrangement. The bearing reaction forces are found to have different orientations, probably caused by the rocking moments brought by the helical teeth (it can be noticed that the differences are more significant on bearings 3 and 4 on the gear shaft because the gear radius, hence the moment of rocking, is larger).

5. Conclusion

In this paper, a model has been presented which couples the global behaviour of the system (shaft vibrations) and the contacts between the gear teeth and those in the journal bearings. Tooth microgeometry including shape modifications and errors is taken into consideration, and the influence of temperature on the properties of the bearing lubricant is also considered. The resulting state equations are solved by a multi-iterative numerical process which simultaneously converges on the DOFs, instant load distributions, and geometries along with the bearing temperatures. The experimental evidence from a sophisticated single-stage test rig with spur and helical gears has been used to assess the validity and the precision of the model. Despite the limited number of DOFs, the experimental and numerical root stresses compare very well for both spur and helical gears and for various bearing centre distances. The tooth critical speeds are correctly positioned, and the associated amplitudes are satisfactory thus validating the proposed model. The average running positions of the shafts within the bearings seem to be correctly simulated, and some differences between the spur and helical gear cases are pointed out probably because of the rocking moments induced by the helix angle. From a general viewpoint, it is confirmed that gears, shafts, and journal bearings are dynamically coupled and that accurate bearing models are required in order to predict tooth critical speeds.

References

[1] D. Dowson, "A generalized Reynolds equation for film lubrication," *International Journal of Mechanical Science*, vol. 4, no. 2, pp. 159–170, 1962.

[2] J. W. Lund, "The stability of an elastic rotor in journal bearings with flexible damped supports," *Journal of Applied Mechanics*, vol. 32, no. 4, pp. 911–918, 1965.

[3] A. Cameron, *The Principles of Lubrication*, Longmans, New York, NY, USA , 1966.

[4] O. Pinkus and B. Sternlight, *Theory of Hydrodynamic Lubrication*, McGraw-Hill, New York, NY, USA, 1971.

[5] J. Frêne, D. Nicolas, B. Degueurce, D. Berthe, and M. Godet, *Lubrification Hydrodynamique—Paliers Et Butées*, Éditions Eyrolles, 1998.

[6] O. Pinkus and D. J. Wilcock, "Thermal effects in fluid film bearings," in *Proceeding of the 6th Leeds-Lyon Symposium on Tribology: Thermal effects on tribology*, pp. 3–23, Mechanical Engineering Publications, 1980.

[7] D. Nicolas, *Les paliers hydrodynamiques soumis à un torseur de forces quelconque [Ph.D. thesis]*, INSA de Lyon, Lyon, France, 1972.

[8] B. Fantino, J. Frene, and J. Du Parquet, "Elastic connecting-rod bearing with piezoviscous lubricant: analysis of the steady-state characteristics," *Journal of lubrication technology*, vol. 101, no. 2, pp. 190–200, 1979.

[9] H. N. Özgüven and D. R. Houser, "Athematical models used in gear dynamics. A review," *Journal of Sound and Vibration*, vol. 121, no. 3, pp. 383–411, 1988.

[10] P. Velex, "Modélisation du comportement dynamique des transmissions par engrenages," in *Comportement Dynamique Et Acoustique Des Transmissions Par Engrenages*, CETIM, Ed., Chapter 2, pp. 39–95, 1993.

[11] G. W. Blankenship and R. Singh, "A new gear mesh interface dynamic model to predict multi-dimensional force coupling and excitation," *Mechanism and Machine Theory*, vol. 30, no. 1, pp. 43–57, 1995.

[12] F. Küçükay, "Dynamic behaviour of high speed gears," in *Proceedings of the 3rd International Conference "Vibrations on Rotating Machinery"*, pp. 81–90, The Institution of Mechanical Engineers, York, UK, September 1984.

[13] R. W. Munro, *The dynamic behaviour of spur gears [Ph.D. thesis]*, Cambridge University, Cambridge, UK, 1962.

[14] P. Velex and M. Maatar, "A mathematical model for analyzing the influence of shape deviations and mounting errors on gear dynamic behaviour," *Journal of Sound and Vibration*, vol. 191, no. 5, pp. 629–660, 1996.

[15] M. Ajmi and P. Velex, "A model for simulating the quasi-static and dynamic behaviour of solid wide-faced spur and helical gears," *Mechanism and Machine Theory*, vol. 40, no. 2, pp. 173–190, 2005.

[16] S. Baud and P. Velex, "Static and dynamic tooth loading in spur and helical geared systems-experiments and model validation," *Journal of Mechanical Design*, vol. 124, no. 2, pp. 334–346, 2002.

[17] S. Theodossiades and S. Natsiavas, "On geared rotordynamic systems with oil journal bearings," *Journal of Sound and Vibration*, vol. 243, no. 4, pp. 721–745, 2001.

[18] C. S. Chen, S. Natsiavas, and H. D. Nelson, "Coupled lateral-torsional vibration of a gear-pair system supported by a squeeze film damper," *Journal of Vibration and Acoustics*, vol. 120, no. 4, pp. 860–867, 1998.

[19] S. Baguet and G. Jacquenot, "Nonlinear couplings in a gear-shaft-bearing system," *Mechanism and Machine Theory*, vol. 45, no. 12, pp. 1777–1796, 2010.

[20] S. M. Rhode and D. F. Li, "A generalized short bearing theory," *Journal of Lubrication Technology*, vol. 102, no. 3, pp. 278–282, 1980.

[21] N. Abdul-Wahed, *Comportement dynamique des paliers fluides - Etude linéaire et non linéaire [Ph.D. thesis]*, INSA Lyon, Lyon, France, 1982.

[22] C. Weber and K. Banaschek, "The deformation of loaded gears and the effect on their load-carrying capacity. Part 5," Tech. Rep. 6, Department of Scientific and Industrial Research, London, UK, 1950.

[23] G. Lundberg, "Elastische Berührung zweier Halbräume," *Forschung auf dem Gebiete des Ingenieurwesens*, vol. 10, no. 5, pp. 201–211, 1939.
[24] D. G. Christopherson, "A new mathematical method for the solution of oil film lubrication problems," *Proceedings of the Institution of Mechanical Engineers*, vol. 146, pp. 126–135, 1941.
[25] Norme et standard, ISO/TR, 15144-1, 2009.

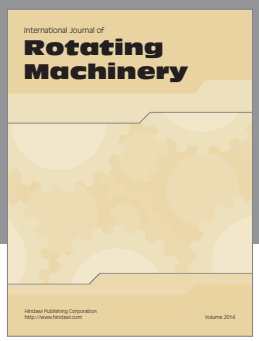

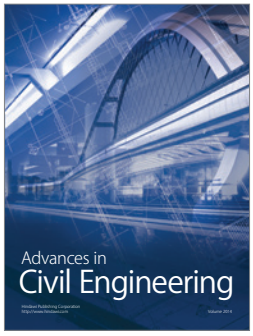

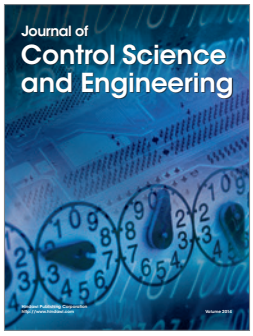

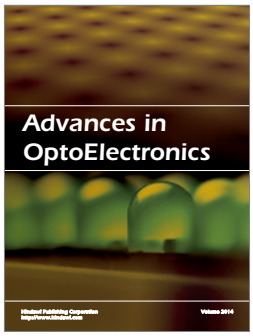

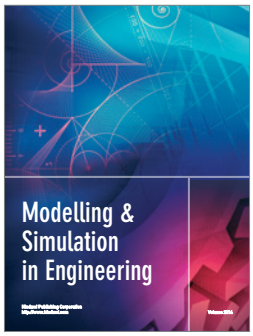

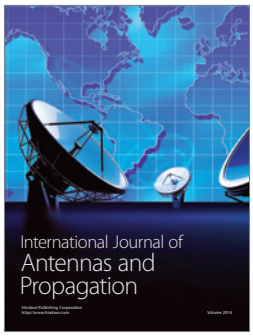

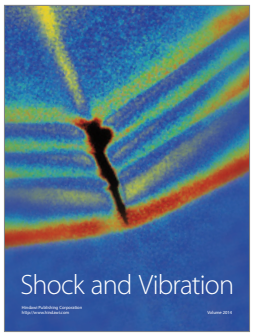

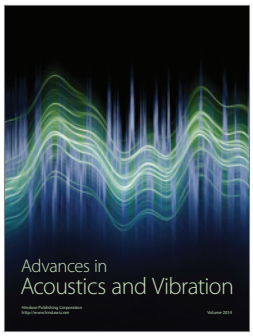

Hindawi

Submit your manuscripts at
http://www.hindawi.com